Journal of Catalysis **196,** 46–55 (2000)
doi:10.1006/jcat.2000.3026, available online at http://www.idealibrary.com on IDEAL®

Different Mechanisms for the Formation of Acetaldehyde and Ethanol on the Rh–Based Catalysts

Yi Wang, Hongyuan Luo, Dongbai Liang, and Xinhe Bao[1]

State Key Laboratory of Catalysis, Dalian Institute of Chemical Physics, The Chinese Academy of Sciences, Dalian 116023, P. R. China

Received February 10, 2000; revised August 4, 2000; accepted August 4, 2000

Different mechanisms for the formation of acetaldehyde and ethanol on the Rh-based catalysts were investigated by the TPR (temperature programmed reaction) method, and the active sites were studied by CO-TPD, TPSR (temperature programmed surface reaction of preadsorbed CO by H_2) and XPS techniques. The TPR results indicated that ethanol and acetaldehyde might be formed through different intermediates, whereas ethanol and methanol might result from the same intermediate. Results of CO-TPD, TPSR, and XPS showed that on the Rh-based catalyst, the structure of the active sites for the formation of C_2-oxygenates is ($Rh^0_x Rh^+_y$)–O–M^{n+} (M = Mn or Zr, $x \gg y$, $2 \le n \le 4$). The tilt-adsorbed CO species is the main precursor for CO dissociation and the precursor for the formation of ethanol and methanol. Most of the linear and geminal adsorbed CO species desorbed below 500 K. Based on the suggested model of the active sites, detailed mechanisms for the formation of acetaldehyde and ethanol are proposed. Ethanol is formed by direct hydrogenation of the tilt-adsorbed CO molecules, followed by CH_2 insertion into the surface CH_2–O species and the succeeding hydrogenation step. Acetaldehyde is formed through CO insertion into the surface CH_3–Rh species followed by hydrogenation, and the role of the promoters was to stabilize the intermediate of the surface acetyl species.

Key Words: **mechanism; acetaldehyde; ethanol; Rh-based catalysts; CO-TPD.**

INTRODUCTION

It is widely accepted (1–4) that the synthesis of C_2-oxygenates on Rh-based catalysts from syngas requires: (a) adsorption and dissociation of H_2 and CO followed by hydrogenation to form CH_x species; (b) CO insertion into surface-alkyl bonds or adsorbed surface carbene group (5) followed by further hydrogenation. However, there are disagreements on the intermediate through which C_2-oxygenates are formed. Many reports (6–12) suggested that surface acetate is the intermediate for the synthesis of C_2-oxygenates, mainly based on the results of IR and isotope labeled experiments. Fukushima *et al.* (13), however, did not accept the acetate as an intermediate and considered that acetate is merely a product of CO hydrogenation. Underwood and Bell (14) also considered that the acetate is present as a spectator species. They suggested that the main intermediate is an acyl species, which is identified by the presence of an IR band at $\sim$1680 cm^{-1}. Nevertheless, most of the reports mentioned above are inclined to believe that acetaldehyde and ethanol are derived from the same intermediate. A different opinion on the mechanism came from Jackson *et al.* (15), who suggested that acetaldehyde and ethanol are derived from different intermediates, and the intermediate for acetaldehyde is the surface acyl group, while that for ethanol is the surface CH_2–O group, which is also the precursor of methanol. In addition, Orita *et al.* (16) also reported that ethanol is not produced via direct hydrogenation of acetaldehyde over the Rh/SiO_2 catalyst. Another different mechanism proposed by Takeuchi *et al.* (17) suggested that ethanol is formed by homologation of methanol.

The active sites for the CO hydrogenation reaction have also been extensively studied. H_2 and CO dissociation, and the succeeding hydrogenation, is generally considered to occur on a fairly large ensemble of Rh^0 atoms (1–3). On the other hand, there are disagreements on the active sites for the CO insertion process. Watson and Somorjai (18, 19) proposed that CO insertion to form C_{2+}-oxygenates occurs on the Rh^+ sites, whereas Katzer *et al.* (20) reported from an XPS study that there was no correlation between the yields of C_2-oxygenates and the number of Rh^+ sites on the catalyst. In recent years, most of the reports agreed that single Rh atom sites are active for CO insertion, whether it is the Rh^0 or the Rh^+ entity (21–23). Moreover, it can be anticipated that the situation will become more complicated when promoters such as Mn, Li, and Zr are added to the Rh/SiO_2 catalyst. Mn is the most extensively studied promoter and is considered to enhance the activity of the Rh-based catalysts through at least three ways: (1) promoting the adsorption and dissociation of CO (2, 3, 24), (2) accelerating the hydrogenation steps (25), and (3) creating new active sites for the CO insertion reaction (26). No matter which interpretation is correct, new active sites do form

[1] To whom correspondence should be addressed.

0021-9517/00 $35.00

on the Rh–Mn/SiO_2 catalyst, which is different from that on the sample without promoters.

In this paper, the TPR (temperature programmed reaction) technique was employed to characterize the Rh-based catalysts, and information about the mechanisms for the formation of C_2-oxygenates can be derived from the results. On the other hand, CO-TPD, XPS, as well as TPSR (temperature programmed surface reaction of preadsorbed CO by H_2) methods were used to investigate the chemical state of the active sites. Based on these results and results from the literature, detailed mechanisms for the formation of acetaldehyde and ethanol, respectively, were suggested, which are different from the mechanisms reported previously.

EXPERIMENTAL

Catalyst preparation. Catalysts were prepared by the incipient wetness impregnation technique by using aqueous solutions of $RhCl_3 \cdot xH_2O$, $Mn(NO_3)_2$, $LiNO_3$, and $Zr(NO_3)_4$. SiO_2 (20–40 mesh, BET area 200 m^2/g, Haiyang Chemicals Plant, China) was used as the support material. Impregnated catalysts were dried in air at 383 K for 4 h, without calcination at a high temperature. The loading amount of active components is in weight percent with respect to the weight of SiO_2.

Characterization of the catalysts by TPR. TPR experiments were performed on a U-type stainless steel reactor with a quartz tube of 6-mm-i.d. attached inside. The reaction zone of about 60 mm length was located in the middle of the reactor and was heated by a cylindrical electric furnace. The temperature of the catalyst bed was controlled by a programmable regulator using a shielded NiCr–NiAl thermocouple attached to the outside of the reactor. The catalyst (about 100 mg) was reduced typically under flowing H_2 (flow rate = 100 ml/min, ambient pressure) at 623 K for 2 h. Afterward, the reduced sample was cooled down in H_2 atmosphere, and syngas (H_2/CO = 2 : 1 volume ratio) was introduced to replace H_2 when the temperature was cooled to RT. The syngas pressure was controlled and adjusted by the pressure regulator in front of the reactor. The flow rate was adjusted by a fine-adjust valve in the outlet. Prior to the running of the TPR experiment, the catalyst bed was swept by syngas for 10 min. The temperature was linearly and continuously increased from RT to 713 K when the TPR experiments was carried out under an ambient syngas pressure. However, when the TPR was carried out under a medium syngas pressure, the temperature was first increased linearly to a given value and kept at this value until the reaction reached the steady state, and then the temperature was increased continually to the next value. This procedure was repeated until the temperature reached 713 K. The heating rate was 13 K/min. The reaction products were analyzed by a computer controlled quadrupole mass spectrometer (Balzers OminiStar). The inlet capillary was mounted directly at the bottom of the reactor. Product distribution was obtained by analyzing the intensities of the corresponding components at their characteristic peaks, which were chosen to avoid possible overlaps in the signals of ion fragments of different molecules.

Characterization of the catalysts by CO-TPD. CO-TPD experiments were carried out on the same setup used for the TPR experiments. The catalyst (100 mg) was reduced first with flowing H_2 (flow rate = 100 ml/min) at a given temperature for 1 h. After this the catalyst bed was swept with He (ultrahigh purity) for 0.5 h at the same temperature, the flow rate of He being 50 ml/min. Then the catalyst was cooled to RT in a He atmosphere and then maintained at RT in He for 0.5 h. The next step was CO adsorption at RT for 0.5 h, and pure CO (ultrahigh purity) was used as the adsorbate. After CO adsorption the catalyst bed was swept again with He for 0.5 h and then the TPD began. TPD was performed in a He atmosphere (flow rate of He = 30 ml/min) with a quadrupole mass spectrometer (QMS, Balzers OmniStar) as a detector to monitor the desorbed species under linearly increasing temperature. The heating rate was 20 K/min.

Characterization of the catalysts by TPSR. The TPSR experiments were carried out as follows: After the catalyst was reduced at 623 K for 2 h, it was cooled down to room temperature and CO was introduced for adsorption at RT for 0.5 h; afterward, pure H_2 was introduced into the reactor instead of CO at ambient pressure. After the catalyst was swept with H_2 for 20 min, the temperature was increased linearly in H_2 and the signals of CO and CH_4 were recorded by the QMS simultaneously.

Characterization of the catalysts by XPS. XPS measurements of the samples after reduction and reaction were completed on a PHI1600 ESCA system. The testing conditions were as follows: radiation source, Mg$K\alpha$, PE = 23 eV; detection area = 0.8 mm^2, pressure in the analysis chamber = 2×10^{-8} Torr. The charging effects were calibrated by the binding energy of C1s (284.5 eV). Before the experiments, the samples were pressed into self-supporting wafers and mounted on the stainless-steel manipulator.

Pretreatment of the samples were carried out as follows: (i) The catalysts were pressed into self-supporting wafers, and then the wafers were put into a specific reactor and labeled in given order. H_2 was introduced into the reactor to reduce the sample wafers at 623 K for 2 h. After this the wafers were sealed into labeled small measuring bottles under an atmosphere of N_2 (high purity), and the sample wafers were then transferred into the vacuum chamber under the same inert atmosphere. All the operations were carefully carried out in order to prevent the catalyst from being exposed to air. (ii) As described above, after the catalyst was reduced, the temperature was decreased to RT.

Then syngas was introduced into the reactor at a flow rate of 30 ml/min, at the same time the temperature was linearly increased to 593 K and maintained at 593 K for 1 h. Then the syngas was switched to N_2 and the catalyst was cooled to RT. The treated sample wafer was finally transferred into the XPS spectrometer under inert atmosphere for detection.

RESULTS AND DISCUSSION

The activity of the Rh–Mn–Li–Zr/SiO_2 catalyst under a syngas pressure of 1.5 MPa is shown in Table 1. It can be seen that CO conversions as well as TOFs of methanol, ethanol, and acetaldehyde increase with reaction temperature below 653 K. Since CO conversion is basically not changed with syngas pressure at a given temperature, the data obtained under different pressures are not listed. This implies that the TOF values are increased with syngas pressure due to the increase of partial pressures of CO and H_2 (positive reaction orders).

Figures 1–3 show the results of TPR on the Rh–Mn–Li–Zr/SiO_2 catalyst under different syngas pressures. The intensities of the ion fragments with mass numbers of 43, 31, and 32 are detected during the TPR process for inspecting the productions of acetaldehyde, ethanol, and methanol, respectively. From Fig. 1 it can be seen that the TPR profiles of acetaldehyde production did not change obviously with the increase of the syngas pressure at a temperature below 650 K. This means that the yield of acetaldehyde was practically uninfluenced by the variation of the syngas pressure in this temperature range. However, the TPR profiles of ethanol production exhibited a rather different tendency with the syngas pressure. As shown in Fig. 2, with the increase of the syngas pressure, the optimum yield of ethanol increased prominently, and the optimum temperature shifted to higher values. At a temperature above 650 K, although the yield of acetaldehyde also exhibited a tendency of increase with syngas pressure, it is much less obvious than the case of ethanol. Figures 4 and 5 show the selectivities of the two oxygenated compounds produced during TPR under different syngas pressures. The curves

TABLE 1

The Activity of the Rh–Mn–Li–Zr/SiO_2 Catalyst under a Syngas Pressure of 1.5 MPa

Temperature (K):		503	553	573	583	593	603	613	623	653
CO conversion (%):		0.98	2.03	2.58	3.01	3.68	4.56	5.09	5.77	11.9
TOF/10^{-2} (s^{-1})	CO	0.77	1.61	2.04	2.38	2.91	3.61	4.03	4.57	9.42
	MeOH	0.08	0.24	0.28	0.31	0.34	0.36	0.38	0.40	0.47
	HAc	0.03	0.12	0.28	0.41	0.50	0.57	0.59	0.64	0.66
	EtOH	0.01	0.23	0.43	0.66	0.88	1.00	1.00	1.10	0.60

Note. GHSV = 10,000 h^{-1}, $H_2/CO = 2.0$ (volume ratio), dispersion of Rh = 0.98.

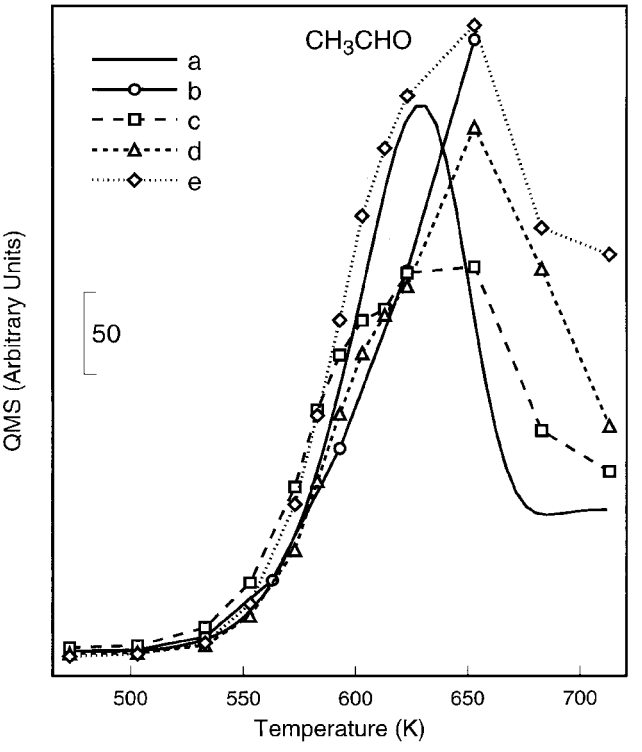

FIG. 1. Acetaldehyde formation on Rh–Mn–Li–Zr/SiO_2 catalyst under various syngas pressures: (a) ambient pressure, (b) 1.0 MPa, (c) 1.5 MPa, (d) 2.3 MPa, (e) 3.5 MPa.

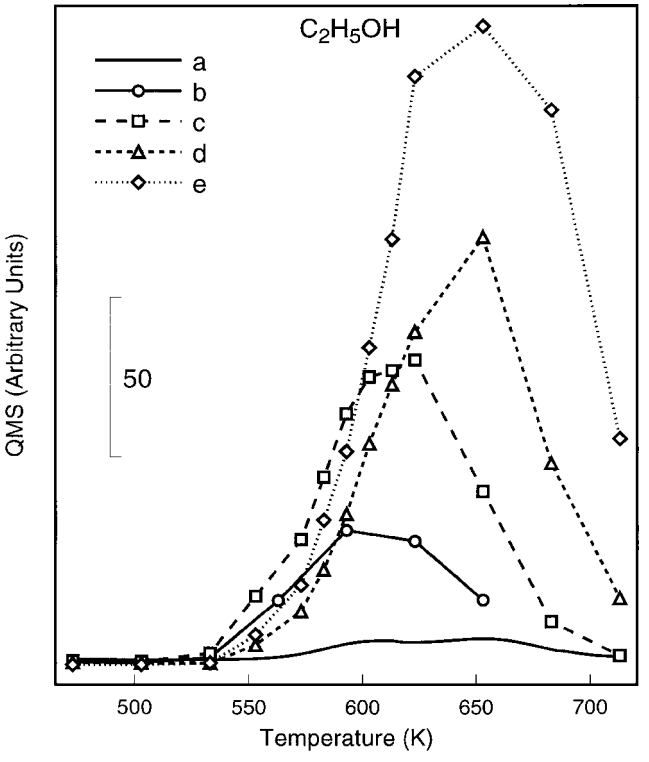

FIG. 2. Ethanol formation on Rh–Mn–Li–Zr/SiO_2 catalyst under various syngas pressures: (a) ambient pressure, (b) 1.0 MPa, (c) 1.5 MPa, (d) 2.3 MPa, (e) 3.5 MPa.

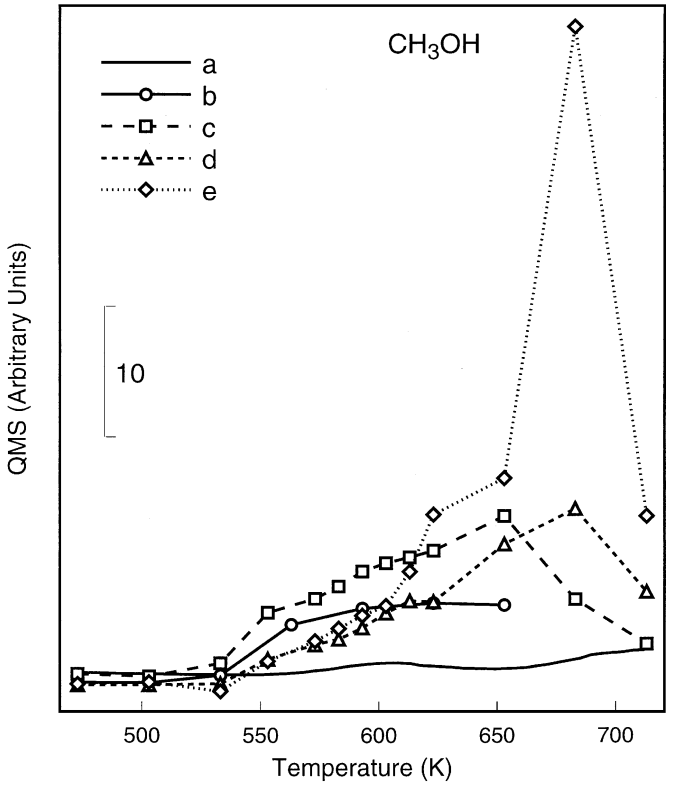

FIG. 3. Methanol formation on Rh–Mn–Li–Zr/SiO_2 catalyst under various syngas pressures: (a) ambient pressure, (b) 1.0 MPa, (c) 1.5 MPa, (d) 2.3 MPa, (e) 3.5 MPa.

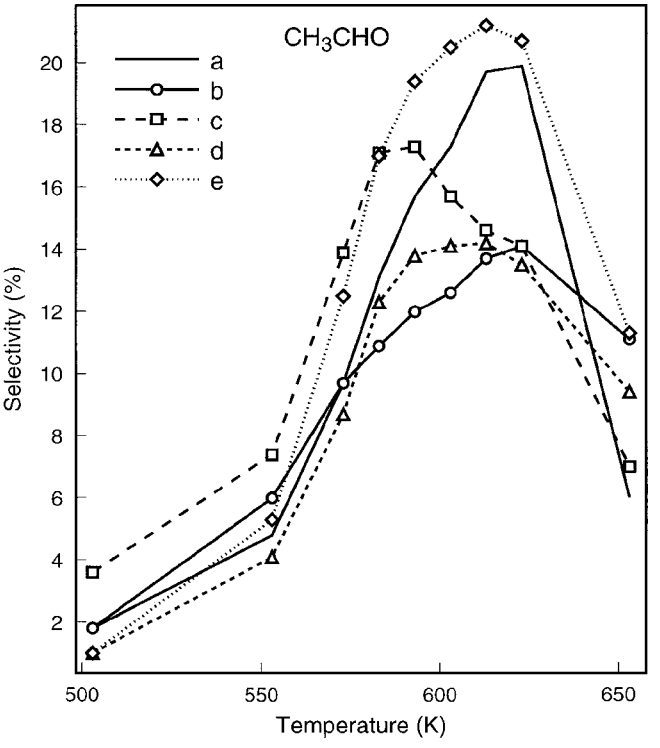

FIG. 4. Selectively of acetaldehyde vs temperature profile on the Rh–Mn–Li–Zr/SiO_2 catalyst for various syngas pressures: (a) ambient pressure, (b) 1.0 MPa, (c) 1.5 MPa, (d) 2.3 MPa, (e) 3.5 MPa.

in Figs. 4 and 5 under different syngas pressures show similar profiles with the corresponding curves in Figs. 1 and 2, respectively. These results implied that acetaldehyde and ethanol might result from different intermediates. This is because if they are derived from the same intermediate, i.e., surface acetyl species, then the amount of both acetaldehyde and ethanol will increase when the CO insertion process is promoted. On the other hand, the TPR profiles of methanol production showed similar tendencies with those of ethanol with the increase of syngas pressure, as evidenced by Figs. 2 and 3, although the temperature dependence of the ethanol yield was slightly different from that of the methanol yield and the yield of methanol was much lower than that of ethanol at various syngas pressures. This indicates that methanol and ethanol may be formed from the same intermediate. This conclusion is confirmed by the results shown in Figs. 5 and 6.

Figure 7 shows the variations of selectivities of the oxygenates compounds with syngas pressures at temperatures of 623 and 653 K, respectively. One can see directly that the selectivities of both ethanol and methanol increase with syngas pressure, whereas that of acetaldehyde is basically unchanged accordingly.

The active sites for the formation of C_2-oxygenates are investigated by the CO-TPD, TPSR, and XPS methods.

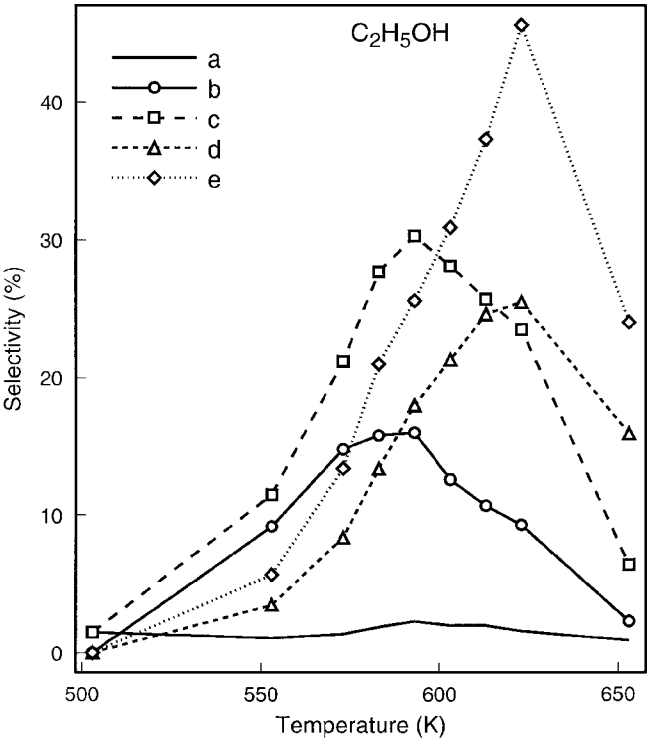

FIG. 5. Selectively of ethanol vs temperature profile on the Rh–Mn–Li–Zr/SiO_2 catalyst for various syngas pressures: (a) ambient pressure, (b) 1.0 MPa, (c) 1.5 MPa, (d) 2.3 MPa, (e) 3.5 MPa.

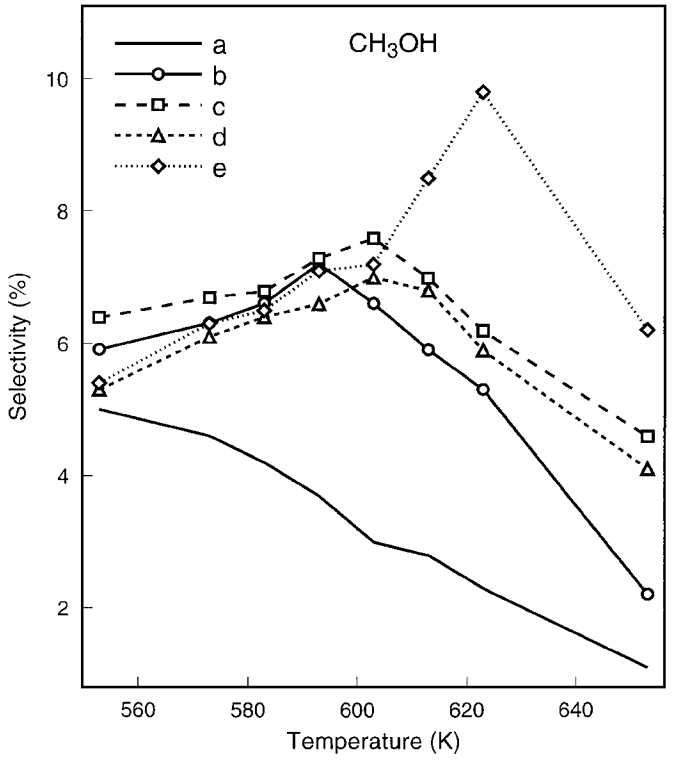

FIG. 6. Selectively of methanol vs temperature profile on the Rh–Mn–Li–Zr/SiO_2 catalyst for various syngas pressures: (a) ambient pressure, (b) 1.0 MPa, (c) 1.5 MPa, (d) 2.3 MPa, (e) 3.5 MPa.

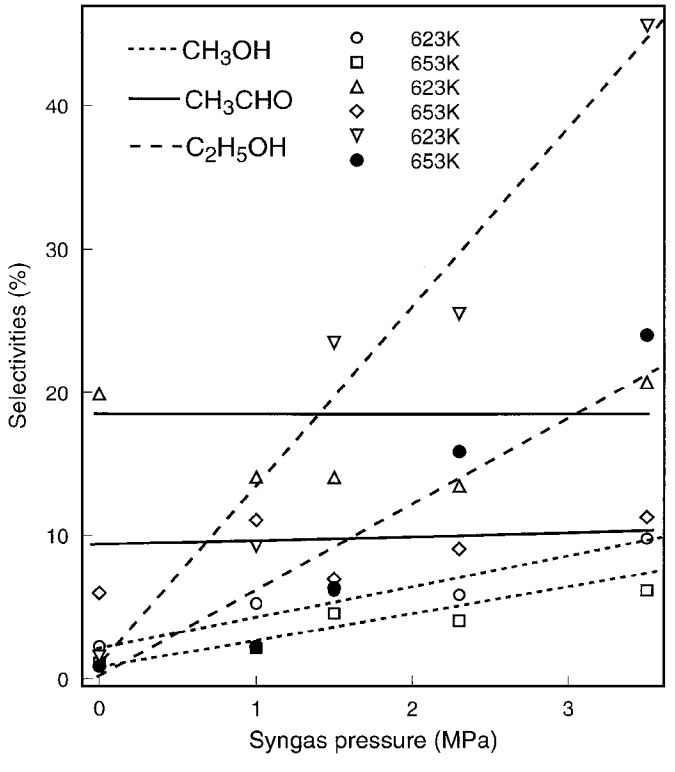

FIG. 7. The variation of selectivities of oxygenated compounds with syngas pressure on Rh–Mn–Li–Zr/SiO_2 catalyst at 623 and 653 K.

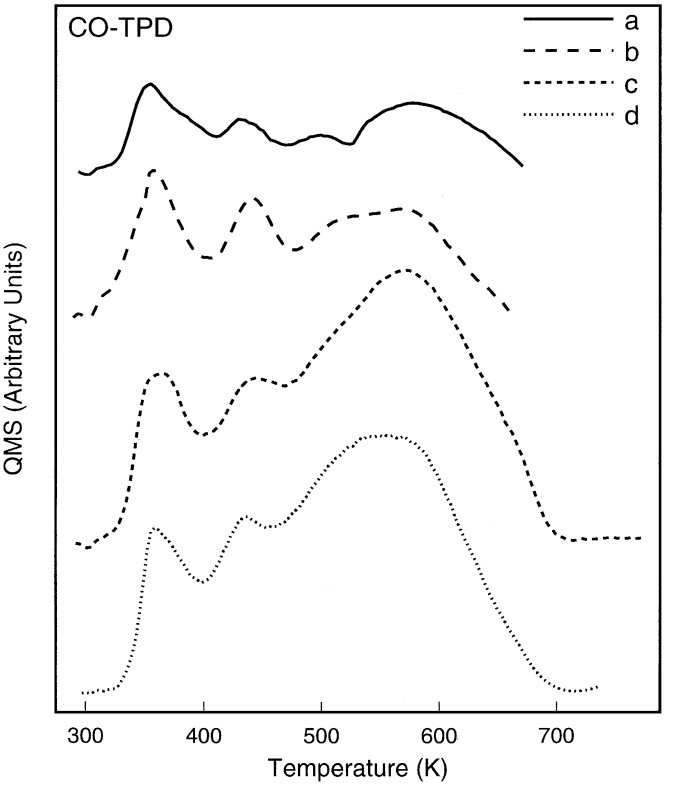

FIG. 8. CO-TPD profiles on various catalysts after reduction at 623 K: (a) Rh/SiO_2, (b) Rh–Mn/SiO_2, (c) Rh–Mn–Li/SiO_2, (d) Rh–Mn–Li–Zr/SiO_2.

Figure 8 shows the CO-TPD results on various catalysts after reduction at 623 K. It can be seen that every TPD profile can be deconvoluted into mainly three peaks, i.e., the peak locates between 300 and 400 K, the peak lies in the temperature range of 400–500 K and the peaks above 500 K. According to IR results reported previously (27), the thermal stability of various types of CO adsorbed on Rh of the highly dispersed Rh/SiO_2 catalyst was in the following order: bridged form > geminal form > linear form. So on the Rh/SiO_2 catalyst, the first desorption peak centered at ca. 350 K should correspond to the linear CO species, and the peak at ca. 425 K may be due to geminal adsorbed CO, which tends to adsorb on isolated Rh atoms. When the desorption temperature exceeds 500 K, the desorption peaks become broader and complicated. We postulate that there may be two CO species desorbing from Rh in this temperature range: One is the bridged form of CO adsorbed on large ensembles of Rh^0 atoms and the other may be a tilt-adsorbed CO species with the C end bonded to the Rh^0 and the O end to the Rh^+ ions. It was reported that the adsorption of CO at room temperature could cause a significant disruption of the Rh crystallites, ultimately leading to isolated Rh^+ ions, which is derived from Rh^0 after oxidized by surface hydroxyls on the support (28). So there does exist a certain amount of Rh^+ ions at the

edge of the Rh^0 clusters and there is the possibility for the formation of the tilt-adsorbed CO species on the Rh/SiO_2 catalyst.

When the promoters such as Mn, Li, and Zr were added to the Rh/SiO_2 catalyst, the adsorption capacity was enhanced obviously, which can be seen from the increase of the total peak area of the CO-TPD profile, as shown in Figs. 8b, 8c, and 8d. On the promoted Rh-based catalysts, the first and the second CO desorption peaks below 500 K are also assigned to the linear and geminal adsorbed CO species, respectively. Comparing with the IR results reported previously (29), it was found that the proportion of geminal form of CO on the CO-TPD profiles is not so much as in the IR spectra, and this may be due to the fact that some of the geminal form of CO can be transferred into other adsorption forms (30) under the desorption conditions. On the promoted catalysts, the desorption peaks at or above 500 K were mainly ascribed to tilt-adsorbed CO, because the bridged CO is difficult to be formed in the presence of promoters such as Mn and Li (29). Since a Rh–Mn mixed oxide was formed in the $Rh–Mn/SiO_2$, and Mn was in close contact with Rh in a state of Mn^{2+} (29), the Mn^{2+} sites exhibited as Lewis acid sites which can accommodate the O end of the CO molecules which have adsorbed on Rh atoms by the C atom. Because Rh was isolated by Mn into small clusters, there were many Rh atoms connecting with Mn^{2+} through the –O– bridges, tilt-adsorbed CO species could be readily formed. In fact, Sachtler *et al.* (22) had reported the existence of a tilt-adsorbed CO species on Rh-based catalysts in the presence of oxophilic promoters such as Mn, Zr, and Ti, based on the observation of a red shift in stretching frequency of the bridging carbonyl. In the present case, we postulate that this species can be derived not only from bridged but also other forms of adsorbed CO, such as linear and geminal forms, leading to a large desorption peak. Because the tilted CO bonded with the surface by both the C and the O atoms, so it is thermally more stable and more difficult to desorb comparing with other species. It can be seen from Fig. 8 that the concentration of the tilt-adsorbed CO species was greatly increased after the addition of Mn, Li, and Zr to the Rh/SiO_2 catalyst as promoters. On the $Rh–Mn–Li/SiO_2$ catalyst, the peak due to the tilt-adsorbed CO is the largest among the four samples. On the Rh–Mn–Li–Zr/SiO_2 catalyst, the peak area was comparable to that of the $Rh–Mn–Li/SiO_2$ sample.

The role of the tilt-adsorbed CO species in the reaction was investigated by TPSR experiments, and the results are shown in Figs. 9 and 10. Figure 9 shows the peaks of CH_4 formation on various catalysts. Since the hydrogenation of carbon into CH_4 is very fast on Rh-based catalysts, the production of CH_4 means that CO dissociates at the same time. That is to say, the dissociation of CO can be detected by inspecting the formation of CH_4. From Fig. 9 it can be seen that on Rh/SiO_2, the peak of CH_4 formation is centered at ca. 550 K, while on $Rh–Mn/SiO_2$, the peak temperature

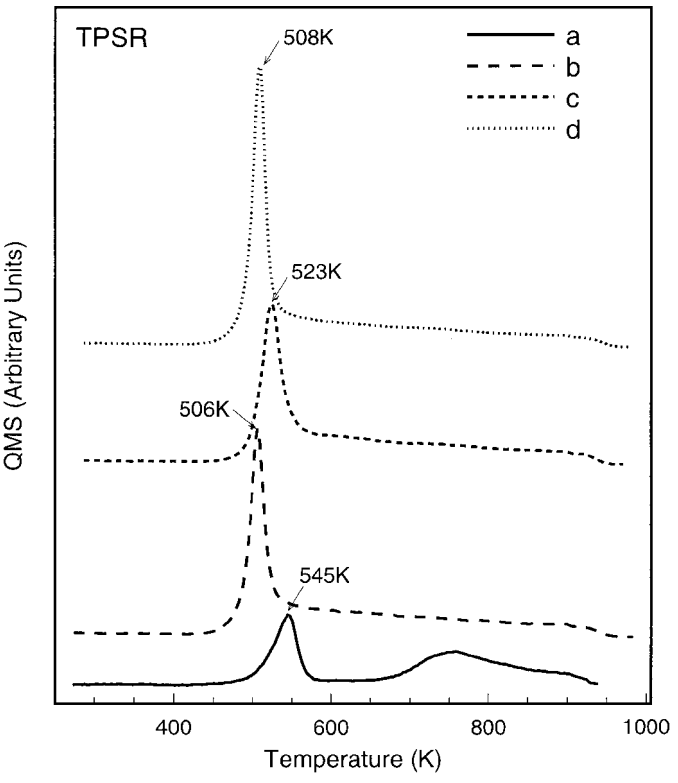

FIG. 9. CH_4 formation profiles on various catalysts during TPSR experiments: (a) Rh/SiO_2, (b) $Rh–Mn/SiO_2$, (c) $Rh–Mn–Li/SiO_2$, (d) Rh–Mn–Li–Zr/SiO_2.

shifted to ca. 500 K. Addition of Li to the $Rh–Mn/SiO_2$ caused the peak temperature to shift to a higher value of ca. 525 K. The peak temperature of the Rh–Mn–Li–Zr/SiO_2 catalyst is almost identical with that of the $Rh–Mn/SiO_2$ sample, i.e., at ca. 500 K. These results indicate that the addition of promoters such as Mn and Zr enhanced the dissociation of CO on the catalyst surface, while introduction of the Li component inhibited CO dissociation to a certain degree. The amount of CH_4 produced on the $Rh–Mn/SiO_2$ and Rh–Mn–Li–Zr/SiO_2 were the largest among the catalysts, whereas on the Rh/SiO_2, the intensity of the peak that centered at ca. 550 K is much lower than that on any other catalysts. The broad peak centered at ca. 750 K in Fig. 9a may be due to the hydrogenation of carbon formed at lower temperatures and transformed to a less active form.

The quantitative results of CO-TPD and TPSR experiments are presented in Table 2. The dispersions of Rh on various catalysts are determined from TPSR results together with the CO-TPD results during the TPSR processes. Assuming that every Rh atom adsorbs one CO molecule and all the CO molecules not desorbing from the catalyst surface can be hydrogenated into CH_4 species. Although CO could get adsorbed on Mn, Zr cations, whereas the amount is very small and can be neglected comparing

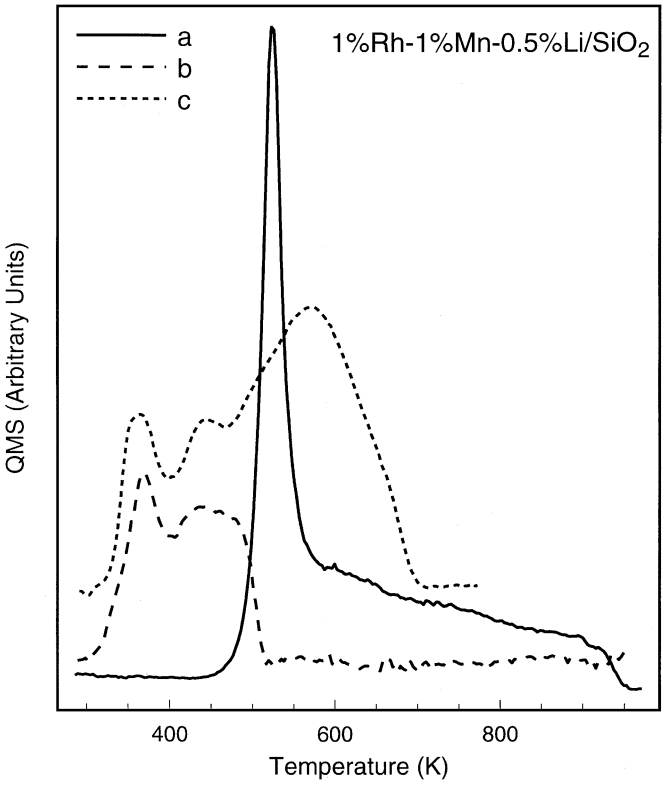

FIG. 10. CO desorption and CH_4 formation on various catalysts during TPSR process on the Rh–Mn–Li/SiO_2 catalyst. (a) CH_4, (b) CO desorbed during TPSR process, (c) CO desorbed during CO-TPD process.

with that adsorbed on Rh and this is evidenced by our previous experiments. On the other hand, on the Rh-based catalysts, there exists a certain amount of gem-dicarbonyl CO adsorbed on the surface. However, there also exists some amount of CO adsorbed in the bridged form, i.e., one CO molecule adsorbed on two Rh atoms. The overestimated stoichiometry of CO : Rh from the gem-dicarbonyl CO can be compensated by the bridged form of CO adsorbed on the catalyst. So the overall stoichiometry of CO : Rh calculated from CO adsorption cannot deviate from the actual value too much. Although the relative populations of gem-dicarbonyl CO and bridged form of CO are different on various catalysts, the error of the stoichiometry of CO : Rh calculated from CO adsorption will not exceed ±10%. Since H_2 spillover might occur on the Rh-based catalysts (29) and there might exist a certain amount of CO which can not desorb from the catalyst surface during the CO-TPD experiments, so the dispersion of Rh cannot be determined by either H_2 adsorption or CO-TPD experiments.

Figure 10 shows the CO-TPD and profiles of CH_4 production on the Rh–Mn–Li/SiO_2 catalyst. It is obvious that CH_4 is formed at the expense of the strongly adsorbed CO species, and most of them were tilt-adsorbed CO molecules having a desorption peak at above 500 K. The same phenomenon can be seen on other catalysts. So it can be concluded that during the TPSR process, the tilt-adsorbed CO dissociated and was eliminated from the surface by hydrogenation. However, most of the linear CO and the geminal form of CO adsorbed on the surface did not dissociate, and desorbed into the gas phase upon heating. The results confirmed the postulate (22) that the tilt-adsorbed CO species is the main precursor for CO dissociation on the catalysts.

The valence state of Rh as well as the promoters was investigated by XPS after *in situ* reduction and reaction. The results are shown in Table 3.

From Table 3 it can be found that the binding energy of the Rh3$d_{5/2}$ peaks are centered at about 306.9–307.3 eV on various catalysts after reduction and reaction. This indicates that Rh existed on the catalyst surface mainly in the metallic state (Rh^0) during both of the processes. There was no or only negligible amounts of Rh^+ on the catalysts. Mn existed in the form of Mn^{2+} or higher valence states (Mn^{3+} and Mn^{4+}) after reduction and reaction, which can be seen from the BE of Mn2$p_{3/2}$. Also, from the BEs of Li2*s* and Zr3$d_{5/2}$, we know that Li existed as Li^+ and Zr existed as Zr^{4+} on the catalyst surfaces after reduction and reaction.

Based on the results of CO-TPD, TPSR, and XPS experiments, the active sites for the formation of C_2-oxygenates on the Rh-based catalysts can be summarized in two aspects: (1) Results of XPS indicated that most of the Rh on Rh-based catalysts existed on the catalyst surface in metallic state (Rh^0). So we can conclude that Rh^0 is active for the

TABLE 2

Quantitative Results of CO-TPD and TPSR Experiments

Catalyst:	Rh/SiO_2	Rh–Mn/SiO_2	Rh–Mn–Li/SiO_2	Rh–Mn–Li–Zr/SiO_2
CO (TPD) (μmol/g_{cat})	10	17	40	38
CH_4 (TPSR) (μmol/g_{cat})	38	60	61	66
CO (TPSR) (μmol/g_{cat})	5.0	33	33	29
Dispersion of Rh (μmol Rh_s/g_{cat})	43	93	94	95

Note. CO (TPD), CO desorbed during CO–TPD; CH_4 (TPSR), CH_4 produced during TPSR; CO (TPSR), CO desorbed during TPSR; the content of Rh is 1 wt% on each catalyst.

TABLE 3

Binding Energies of Various Components on the Rh-Based Catalysts after Reduction and Reaction

Samples	Testing conditions	Binding energies (eV)			
		Rh3$d_{5/2}$	Mn2$p_{3/2}$	Li2s	Zr3$d_{5/2}$
1%Rh/SiO_2	After reduction	307.0			
	After reaction	307.2			
1%Rh–1%Mn/SiO_2	After reduction	306.9	641.9		
	After reaction	306.9	641.9		
1%Rh–1%Mn–0.5%Li/SiO_2	After reduction	307.0	641.9	55.2	
	After reaction	307.0	641.9	55.7	
1%Rh–1%Mn–0.5%Li–0.8%Zr/SiO_2	After reduction	307.3	642.1	55.1	182.9
	After reaction	307.0	642.2	55.4	183.0

formation of C_2-oxygenates. However, the possibility that Rh^+ plays a role in CO insertion to form C_2-oxygenates cannot be ruled out completely. There are reports (18, 19) in which Rh^+ was considered as active sites for the formation of C_2-oxygenates. The different results obtained in XPS experiments might be due to different catalyst preparation methods, different composition of the catalysts, and different pretreatment of the catalysts. In fact, Rh^+ might exist on the catalyst during reaction as an unstable intermediate derived from Rh^0 after oxidation by O atoms generated by CO dissociation. It is well known that CO chemisorbs on Rh^0 at room temperature and leads to isolated Rh^+ species that change into Rh^0 after CO desorption. (2) The geometric structure of the active sites can be proposed as $(Rh_x^0Rh_y^+)$–O–M^{n+}, where $x \gg y$, $M =$ Mn or Zr, $2 \le n \le 4$. The suggestion of such a structure is based on CO-TPD, XPS, as well as our previously EPR results (29). The existence of the tilt-adsorbed CO species on the promoted Rh/SiO_2 catalysts implied that most of the promoter ions (such as Mn^{2+} or Zr^{4+}) are in close contact with Rh. EPR results indicated that on the Rh–Mn/SiO_2 catalyst, Rh–Mn mixed oxide is formed on the as-prepared sample, and Mn is in close contact with Rh through the –O– bridge bonds (29). The present XPS results indicate that during reduction and reaction, Mn exists in the form of Mn^{2+} or higher valence states (Mn^{3+} and Mn^{4+}). Both of the CO-TPD and TPSR results indicated that Zr exhibits a similar promoting effect as Mn does. Accordingly, we suggest the structure of the active site as described above.

Based on the structure of the active sites suggested above, the tilt-adsorbed CO can be described as follows:

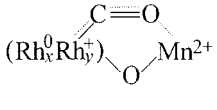

The TPSR results indicate that this configuration of CO species is the main precursor of CO dissociation. However, we postulated that this tilt-adsorbed CO species was not only the precursor of CO dissociation, but also the precursor for methanol and ethanol formation. From CO-TPD results it can be seen that under the reaction temperature (about 593 K) there must be a certain amount of the tilted CO species adsorbed on the catalyst without dissociation. The undissociated CO can be directly hydrogenated into the CH_2–O species, which is the precursor of methanol. This is consistent with the mechanism of methanol formation on Rh-based catalyst (31). Ethanol can be formed through CH_2 insertion into the CH_2–O species. This mechanism is suggested based on the TPR results which showed that methanol and ethanol might be formed through the same intermediate, as described in Fig. 11.

The TPR results also indicated that acetaldehyde and ethanol are not formed through the same intermediate. We suggest that acetaldehyde is formed through CO insertion into the surface CH_x–Rh bond, and the active sites for the insertion is considered to be the isolated Rh atom, as described in the literature (21–23). The addition of promoters such as Mn and Li to Rh/SiO_2 enhanced the dispersion of Rh obviously, as shown in Table 2, and isolated Rh atoms

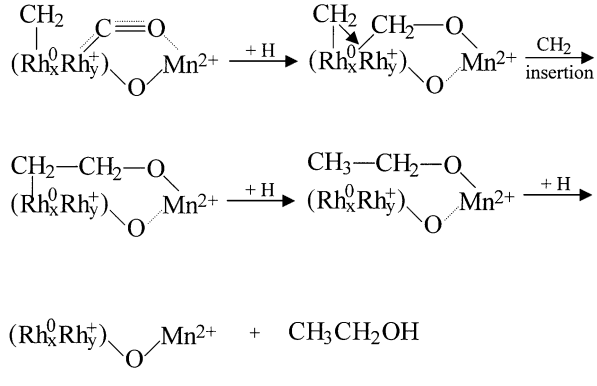

FIG. 11. The mechanism of ethanol formation on the Rh–Mn/SiO_2 catalyst.

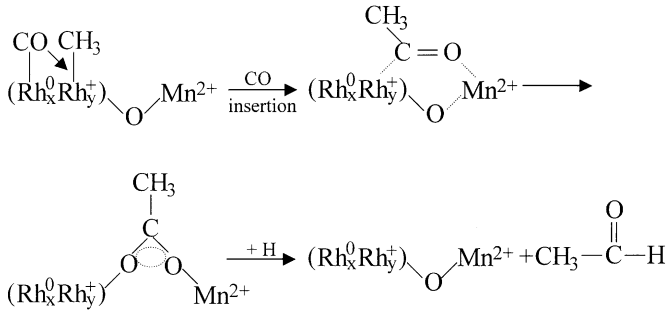

FIG. 12. The mechanism of acetaldehyde formation on the Rh–Mn/SiO_2 catalyst.

are increased. However, the increase of selectivity to acetaldehyde after adding the promoters cannot be simply ascribed to the increase in Rh dispersion, since the extent to which the dispersion of Rh was increased was very small comparing with the increase of selectivity of acetaldehyde by adding the promoters. Wang *et al.* (24) investigated the dispersion of Rh after addition of the promoters such as Mn and Li, and the results indicated that on their Rh/SiO_2 catalyst, the dispersion of Rh was 0.64, whereas the dispersion increased to 0.70 and 0.77 after adding comparable amounts of Mn and Li, respectively. The discrepancy of our results with theirs may be due to the difference in Rh content and catalyst preparation conditions. We consider that the existence of promoters such as Mn and Li stabilizes the intermediate for the formation of acetaldehyde; i.e., the surface acetyl species is stabilized by interacting with the promoter, as shown in Fig. 12.

Figure 12 implies that the surface acetyl species is formed at the edge of a Rh cluster and interacts with the Mn^{2+} ions, leading to the formation of a surface acetate group which is more stable than the acetyl species. The hydrogenation of the surface acetate group results in the formation of acetaldehyde. It can also be inferred from Fig. 12 that only the Rh atoms at the perimeter of the clusters are active for C_2-oxygenates formation. In fact, the Mn^{2+} ions can be substituted by Zr^{4+} or other oxophilic ions, which exhibit similar promoting effect. Bowker (32) suggested that there are four kinds of acetate groups on the promoted Rh-based catalysts during the reaction, but only those in contact with both the Rh atom and the promoter oxide are active for the formation of C_2-oxygenates. This is consistent with our suggestion. We also proposed that the hydrogenation of surface acetate group yields mainly acetaldehyde, although there may be a small amount of ethanol formed simultaneously. On the other hand, the main function of Li as a promoter is considered to adjust the hydrogenation capacity as well as the selectivity of the catalyst (33). Further investigations on the role of Li should be carried out in the future.

From the mechanisms described above, it can be seen that the formation of ethanol is strongly dependent on the existence of promoters, since the formation of tilt-adsorbed CO requires both the Rh and the promoter ions to locate the CO molecules. On the other hand, the formation of acetaldehyde is relatively independent of the promoters, since the direct CO insertion only requires isolated Rh atoms. In fact, the necessity of the promoters for the formation of ethanol was confirmed by the results of Nonneman *et al.* (34), who found that trace amounts of impurities such as Fe, Na, and other components existing inherently on the support (silica) exhibited prominent promoting effects for the formation of C_2-oxygenates such as ethanol and acetaldehyde. If the SiO_2 support was purified to a very high degree, then on the Rh/SiO_2 catalyst no ethanol could be formed but the activity for acetaldehyde production remained to a certain extent. This might be another evidence that ethanol and acetaldehyde are formed through different mechanisms.

The mechanisms that suggested by us are different from most of the mechanisms suggested previously in which acetaldehyde and ethanol were considered to be formed through the same intermediate. The mechanism for the formation of ethanol is similar to that proposed by Jackson *et al.* (15), whereas that for the formation of acetaldehyde was different from that suggested by them, who believed that acetaldehyde is formed through CH_2 insertion into the surface–CO bonds followed by hydrogenation. The concept that the tilt-adsorbed CO species is the precursor of ethanol has never been reported previously.

SUMMARY AND CONCLUSIONS

There are linear, geminal, bridged, and tilted forms of CO adsorbed on the surfaces of various Rh-based catalysts. Addition of promoters such as Mn, Li, and Zr increased the amount of tilt-adsorbed CO species, and it became the main CO species adsorbed on these promoted catalysts. The tilted CO was the main precursor for dissociation. Addition of promoters such as Mn and Zr enhanced the dissociation of CO, whereas introduction of the Li component inhibited the CO dissociation to a certain degree.

The active sites for the formation of C_2-oxygenates on the promoted catalysts are considered to be $(Rh^0_x Rh^+_y)$–O–M^{n+} (M = Mn or Zr, $x \gg y$, $2 \le n \le 4$). The tilted CO species is suggested to be not only the precursor for CO dissociation but also the precursor for methanol and ethanol formation. Ethanol is formed by direct hydrogenation of the tilted CO molecules, followed by CH_2 insertion into the surface CH_2–O species and the succeeding hydrogenation. Acetaldehyde is formed through a mechanism different from that of ethanol. The first step for acetaldehyde formation is CO insertion into the surface CH_3–Rh species and yields the surface acetyl group, and this step is considered to have occurred at the perimeter of the Rh clusters. The next step is the stabilization of the acetyl group by forming a surface acetate group contacting with both the Rh atom

and the promoter oxide, followed by the hydrogenation of the acetate species.

ACKNOWLEDGMENTS

We thank the National Natural Science Foundation of China as well as BASF Chemical Company for their financial supports of this project.

REFERENCES

1. Sachtler, W. M. H., *in* "Proceedings, 8th International Congress on Catalysis, Berlin, 1984" (G. Ertl. Ed.), Vol. 1, p. 151. Dechema, Frankfurt-am-Main, 1984.
2. Ichikawa, M., Fukushima, T., and Shikakura, K., *in* "Proceedings, 8th International Congress on Catalysis, Berlin, 1984" (G. Ertl, Ed.), Vol. 2, p. 69. Dechema, Frankfurt-am-Main, 1984.
3. Sachtler, W. M. H., Shriver, D. F., Hollenberg, W. B., and Lang, A. F., *J. Catal.* **92**, 429 (1985).
4. Ichikawa, M., and Fukushima, T., *J. Chem. Soc. Chem. Commun.* 321 (1985).
5. Takeuchi, A., and Katzer, J. R., *J. Phys. Chem.* **86**, 2438 (1982).
6. Orita, H., Naito, S., and Tamaru, K., *J. Phys. Chem.* **89**, 3066 (1985).
7. Orita, H., Naito, S., and Tamaru, K., *J. Chem. Soc., Chem. Commun.* 150 (1984).
8. Lee, G. V. D., Bastein, A., Boogert, J. V. D., Schuller, B., Luo, H., and Ponec, V., *J. Chem. Soc. Faraday 1* **83**, 2103 (1987).
9. Bastein, T., Ph.D. thesis, University of Leiden, The Netherlands, 1988.
10. Koerts, T., Welters, W., Van Santen, R., Nonneman, L., and Ponec, V., *Proceedings, Natural Gas Conversion Symposium*, Oslo, August 1990.
11. (a) Efstathiou, A., and Bennett, C. O., *J. Catal.* **120**, 118 (1989); (b) Efstathiou, A., and Bennett, C. O., *J. Catal.* **120**, 137 (1989).
12. Tau, L. M., Robinson, R., Ross, R. D., and Davis, B. H., *J. Catal.* **105**, 335 (1987).
13. Fukushima, T., Arakawa, M., and Ichikawa, M., *J. Chem. Soc. Chem. Commun.* 729 (1985).
14. Underwood, R. P., and Bell, A. T., *J. Catal.* **111**, 325 (1988).
15. Jackson, S. D., Brandreth, B. J., and Winstanbey, D., *J. Catal.* **106**, 464 (1987).
16. Orita, H., Naito, S., and Tamaru, K., *J. Catal.* **90**, 183 (1984).
17. Takeuchi, A., and Katzer, J. R., *J. Catal.* **82**, 474 (1983).
18. Watson, P. R., and Somorjai, G. A., *J. Catal.* **72**, 347 (1981).
19. Watson, P. R., and Somorjai, G. A., *J. Catal.* **74**, 282 (1982).
20. Katzer, J. R., Sleight, A. W., Gagardo, F., Michel, J. B., Gleason, E. F., and McMillan, S., *Faraday Discuss. Chem. Soc.* **72**, 121 (1981).
21. Chuang, S. S. C., and Pien, S. I., *J.Catal.* **138**, 536 (1992).
22. Sachtler, W. M. H., and Ichikawa, M., *J. Phys. Chem.* **90**, 4752 (1986).
23. Chuang, S. S. C., and Pien, S. I., *J. Catal.* **135**, 618 (1992).
24. Wang, H. Y., Liu, J. P., Fu, J. K., and Tsai, K. R., *Chin. J. Mol. Catal.* **7**, 252 (1993).
25. Van Den Berg, F. G. A., Glezer, J. H. E., and Sachtler, W. M. H., *J. Catal.* **93**, 340 (1985).
26. Trevino, H., Hyeon, T., and Sachtler, W. M. H., *J. Catal.* **170**, 236 (1997).
27. Ugo, R., *Catal. Rev.* **11**, 255 (1975).
28. Basu, P., Panayotov, D., and Yates, J. T., *J. Phys. Chem.* **91**, 3133 (1987).
29. Wang, Y., Song, Z., Ma, D., Luo, H. Y., Liang, D. B., and Bao, X. H., *J. Mol. Catal. A* **149**, 51 (1999).
30. Yates, D. J. C., Murrel, L. L., and Prestrige, E. B., *J. Catal.* **57**, 41 (1979).
31. Takeuchi, A., and Katzer, J. R., *J. Phys. Chem.* **85**, 937 (1981).
32. Bowker, M., *Catal. Today.* **15**, 77 (1992).
33. Wang, Y., Song, Z., Ma, D., Luo, H. Y., Liang, D. B., and Bao, X. H., *Stud. Surf. Sci. Catal.*, in press.
34. Nonneman, L. E. Y., Bastein, A. G. T. M., and Ponec, V., *Appl. Catal.* **62**, L23 (1990).